Water Research 241 (2023) 120150

Contents lists available at ScienceDirect

Water Research

journal homepage: www.elsevier.com/locate/watres

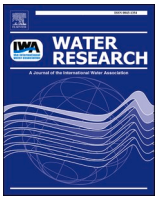

Mercury isotope compositions in seawater and marine fish revealed the sources and processes of mercury in the food web within differing marine compartments

Shaochen Yang [a], Ping Li [b], Kaifeng Sun [c], Nan Wei [c], Jinling Liu [a,*], Xinbin Feng [b]

[a] Hubei Key Laboratory of Critical Zone Evolution, School of Earth Sciences, China University of Geosciences, Wuhan 430074, China
[b] State Key Laboratory of Environmental Geochemistry, Institute of Geochemistry, Chinese Academy of Sciences, Guiyang 550081, China
[c] South China Institute of Environmental Sciences, Ministry of Ecology and Environment of the People's Republic of China, Guangzhou 510655, China

ARTICLE INFO

Keywords:
Marine compartments
Seawater
Marine fish
Mercury sources
Isotope fractionation

ABSTRACT

Anthropogenic activities and climate change have significantly increased mercury (Hg) levels in seawater. However, the processes and sources of Hg in differing marine compartments (e.g. estuary, marine continental shelf (MCS) or pelagic area) have not been well studied, which makes it difficult to understand Hg cycling in marine ecosystems. To address this issue, the total Hg (THg) concentration, methylmercury (MeHg) concentration and stable Hg isotopes were determined in seawater and fish samples collected from differing marine compartments of the South China Sea (SCS). The results showed that the estuarine seawater exhibited substantially higher THg and MeHg concentrations than those in the MCS and pelagic seawater. Significantly negative δ^{202}Hg (−1.63‰ ± 0.42‰) in estuarine seawater compared with that in pelagic seawater (−0.58‰ ± 0.08‰) may suggest watershed input and domestic sewage discharge of Hg in the estuarine compartment. The Δ^{199}Hg value in estuarine fish (0.39‰ ± 0.35‰) was obviously lower than that in MCS (1.10‰ ± 0.54‰) and pelagic fish (1.15‰ ± 0.46‰), which showed that relatively little MeHg photodegradation occurred in the estuarine compartment. The Hg isotope binary mixing model based on Δ^{200}Hg revealed that approximately 74% MeHg in pelagic fish is derived from atmospheric Hg(II) deposition, and over 60% MeHg in MCS fish is derived from sediments. MeHg sources for estuarine fish may be highly complex (e.g. sediment or riverine/atmospheric input) and further investigations are warranted to clarify the contribution of each source. Our study showed that Hg stable isotopes in seawater and marine fish can be used to identify the processes and sources of Hg in different marine compartments. This finding is of great relevance to the development of marine Hg food web models and the management of Hg in fish.

1. Introduction

Mercury (Hg) is a globally distributed pollutant, and its toxicity depends on its chemical form (Mason et al., 2012). Methylmercury (MeHg) is one of the organic forms of Hg that can cause long-term developmental delays in children and cardiovascular negative effects in adults (Bellanger et al., 2013). MeHg is mainly formed by anaerobic microbial methylation of inorganic Hg (IHg) and can biomagnify at each successive trophic level (TL) in aqueous food webs, which subsequently makes predatory fish exhibit concentrations that are approximately a million times higher than those in the water column (Krabbenhoft and Sunderland, 2013). Marine ecosystems are exposed to a wide variety of Hg sources owing to their exposure and proximity to the atmosphere, land, and rivers (Croizier et al., 2020). Anthropogenic Hg emissions into the atmosphere are 5- to 10-fold higher than natural emissions and have resulted in surface seawater concentrations of Hg that are approximately three times higher than pre-anthropogenic levels (Lamborg et al., 2014). Watershed erosion can enhance the transport of large amounts of terrestrial Hg to coastal seas (Mason et al., 2012), and may be responsible for a large percentage of the riverine Hg discharge into the ocean (Liu et al., 2021a); for instance, high-flow events under climate change can strongly contribute to this issue. Excessive Hg input into marine ecosystems may be directly linked to an increased risk of MeHg exposure through marine fish consumption (Krabbenhoft and Sunderland, 2013; Schartup et al., 2020). To better understand the health risks associated with MeHg intake and to predict future MeHg levels in marine fish in

* Corresponding author.
E-mail address: liujinling@cug.edu.cn (J. Liu).

https://doi.org/10.1016/j.watres.2023.120150
Received 3 February 2023; Received in revised form 25 May 2023; Accepted 28 May 2023
Available online 30 May 2023

future, growing efforts are needed to investigate the potential behaviour of Hg in seawater and organisms in marine ecosystems. However, variations in Hg sources, mobility and underlying processes in differing marine compartments (e.g., estuary, marine continental shelf (MCS) or pelagic zone) are complicated and have not been exhaustively studied (Mason et al., 2012; Maurice et al., 2021; Senn et al., 2010); this lack of knowledge renders comprehensively understanding Hg behaviour and bioaccumulation in marine ecosystems challenging (Perrot et al., 2019).

In recent studies, Hg stable isotopes are being increasingly used to obtain information for deciphering the environmental sources and processes of Hg in natural ecosystems in recent studies (Blum et al., 2014; Kwon et al., 2020). The kinetics processes and equilibrium exchange of Hg can be delineated through mass-dependant fractionation (MDF) and expressed as δ^{202}Hg (Kritee et al., 2009; Wiederhold et al., 2010; Zheng et al., 2007). Moreover, Hg is susceptible to mass-independent fractionation (MIF) in the environment (Bergquist and Blum, 2007). The MIF of Hg generally occurs through photochemical processes (e.g., MeHg photodegradation and Hg^{2+} photooxidation), including odd-MIF and even-MIF (Tsui et al., 2020a). Odd-MIF value is expressed as Δ^{199}Hg or Δ^{201}Hg, whereas even-MIF value is denoted as Δ^{200}Hg (Bergquist and Blum, 2007). The utilization of the Hg isotope composition in water samples for Hg source identification in the environment has gained considerable importance; recent works have developed methods, such as nanogold-decorated silica monoliths absorption (Huber et al., 2015), chlorine-impregnated activated carbon preconcentration (Li et al., 2019), and sulfide coprecipitation (Liu et al., 2021b) to accurately detect Hg isotope values in natural water with ultratrace levels of Hg. Previous observations have shown that the Hg isotope composition in freshwater can be used to elucidate Hg deposition pathways in forested watersheds and rivers (Jiskra et al., 2017; Tsui et al., 2020b; Woerndle et al., 2018). Besides, Jiskra et al. (2021) used Hg isotopes and found that Hg in seawater can be explained by the mixing of 42% atmospheric Hg(II) gross deposition and 58% Hg(0) gross uptake. Despite these findings, the variations in Hg isotopes in seawater from most marine compartments remain poorly understood. Consequently, investigating Hg isotope characteristics in seawater from differing marine compartments may provide novel insights into the fate of marine Hg and global Hg cycling.

Furthermore, because most of the Hg in marine fish accumulates as MeHg, finding links between Hg isotopes in marine fish and environmental media (e.g. water column or sediment) can help identify the sources and behaviour of MeHg in marine food webs (He et al., 2023). Gehrke et al. (2011) found a correlation relationship between δ^{202}Hg between in coastal sediment and in fish in San Francisco (SF) Bay and proposed that MeHg was mainly generated from local sediments. Given the absence of MIF during most trophic transfer processes, Δ^{199}Hg values in marine organisms has been demonstrated to be an effective tracer for indicating the biogeochemical processes and production sites of MeHg in seawater and sediment (Blum et al., 2013; Madigan et al., 2018; Maurice et al., 2021; Perrot et al., 2019; Sun et al., 2020). Δ^{200}Hg value is presumed to be exclusively generated by upper tropospheric and stratospheric photochemical reactions; it is therefore identified as a conservative tracer for atmospheric Hg deposition pathways in the environment (Fu et al., 2021; He et al., 2023). Consequently, we hypothesised that a combination of three-dimensional Hg isotope characteristics (δ^{202}Hg, Δ^{199}Hg, and Δ^{200}Hg) in marine fish, seawater, and coastal sediments could reveal the information on Hg behaviour in the environment within differing marine compartments.

The South China Sea (SCS) is the largest semienclosed sea in the western tropical Pacific Ocean around developing Asian countries. It contains a variety of complex ecosystems and is vital in terms of global seafood production (Liu et al., 2014). In this study, we investigated total Hg (THg), MeHg concentrations, and Hg isotope characteristics in seawater and marine fish collected from estuarine, MCS and pelagic zones of the SCS. Carbon (δ^{13}C) and nitrogen (δ^{15}N) isotope ratios were also tested to determine the primary dietary sources, TL, and geographical differences in these fish (Lepak et al., 2022). This study aimed to use Hg isotopes to investigate the differences in Hg sources in seawater and marine fish of differing marine compartments and to identify the underlying processes of Hg in marine food webs, so as to develop new insights into Hg biogeochemical cycling in marine ecosystems.

2. Materials and methods

2.1. Study areas and samples collection

A total of 31 seawater and 89 wild marine fish samples were collected from the Pearl River Estuary (PRE, estuarine area, 24 seawater samples, and 31 marine fish samples), Hainan Island (HNI, MCS area, 2 seawater samples, and 24 marine fish samples), and Xisha Island (XSI, pelagic zone, 5 seawater samples, and 34 marine fish samples) in the SCS (Fig. 1) from July 2021 to August 2021. Details of the seawater sampling data (sampling date, longitude, and latitude) are provided in Table S1. Seawater samples were collected using an automatic water sampler (GHY−QCC15–10 L, China). Approximately 100 mL of seawater from each sampling site was filtered with a 0.45 μm filter membrane and acidified with 0.2 mL ultrapure HNO_3 (65%, v/v), then stored in acid-washed Teflon bottles at 4 °C before THg analysis as described in our previous work (Yang et al., 2022). Seawater for MeHg analysis was also filtered by membrane and preserved with H_2SO_4 (9 mol/L, 0.2 mL for a 100 mL sample). In addition, 9 seawater samples (4 samples from the estuary, 2 samples from the MCS, and 3 samples from the pelagic zone) were selected to detect the Hg isotope composition, 10 L were collected, filtered through membrane and acidified with 20 mL ultrapure HNO_3 (65%, v/v), finally stored in the dark prior to isotope analysis. (Li et al., 2019; Xia et al., 2022). Fish samples from the PRE were collected through trawling, whereas those from the HNI and XSI were collected through sea-fishing voyages. The collected fish were preserved at −20 °C in ice boxes and transported to the laboratory, where the species, weight, and lengths of each fish were recorded (Table S2). Muscle tissues were isolated from the fish samples, lyophilised, subjected to moisture content measurement, homogenised using a pulveriser, and finally stored at 4 °C. The average moisture content for all fish samples was 80%; the details of the moisture content for each sample are given in Table S2.

2.2. THg and MeHg analysis

THg and MeHg concentrations in seawater and fish samples were detected using cold vapour atomic fluorescence spectroscopy (CVAFS, Brooks Rand Model III). THg in the seawater samples was detected via BrCl oxidation, $SnCl_2$ reduction, and dual amalgamation combined with CVAFS measurements. MeHg in the seawater samples was detected using distillation, aqueous phase, ethylation, GC separation and CVAFS analysis following the method of Fu et al. (2010). The detection limits of THg and MeHg for seawater samples were 0.1 ng·L^{-1} and 0.009 ng·L^{-1}, respectively. Based on those detection limits, 30 mL and 45 mL of each seawater samples were used to complete the THg and MeHg concentration analyses, respectively. The deviations in THg and MeHg in the duplicate seawater samples were < 10%. For THg in fish samples, about 0.2 g fish tissue was digested with 5 mL HNO_3 (65%, v/v) at 95 °C for 3 h, and then Hg concentrations were determined by the CVAFS method as described in our previous work (Yang et al., 2022). For MeHg in fish samples, approximately 0.1 g of samples was digested in 25% HNO_3 at 60 °C for 12 h; subsequently, MeHg concentrations were measured via aqueous ethylation, purge, trap, and gas chromatography CVAFS detection method, with a 0.3 ng·g^{-1} limit of detection. The deviations in the duplicate fish samples were < 15%. The THg and MeHg concentration recoveries (%) in certified reference materials (CRMs) were 91% and 89% (TORT 3, $n = 11$), respectively. THg and MeHg concentrations in fish samples were expressed as dry weights.

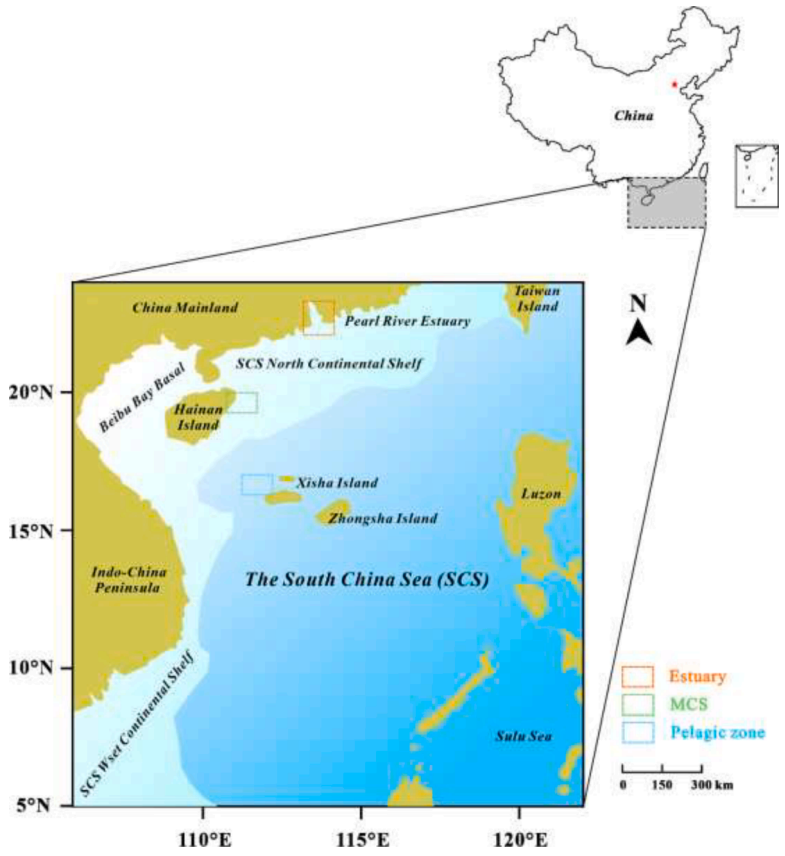

Fig. 1. Study areas in the South China Sea (SCS) in this work. The orange, green and blue square dashed lines surrounding the Pearl River estuary (estuary), Hainan Island (marine continental shelf), and Xisha Island (pelagic zone) are the sampling areas.

2.3. C and N isotope analysis

C ($\delta^{13}C$) and N ($\delta^{15}N$) stable isotope values in the fish samples were determined using a stable isotope instrument (ThermoFisher, MAT253, USA). Ground fish tissue was packed in a tin capsule for C (approximately 0.05 mg) and N (approximately 0.5 mg) stable isotopic measurements. The $\delta^{13}C$ and $\delta^{15}N$ isotopes were measured following established methodologies as documented in prior research and expressed as ‰ (Kim et al., 2015; Yang et al., 2022). The quality control of $\delta^{13}C$ and $\delta^{15}N$ isotope measurements was performed using certified recovery materials $C-3$ ($\delta^{13}C = -24.750‰$) and $N-1$ ($\delta^{15}N = 0.417‰$)) of the International Atomic Energy Agency. Variations in both $\delta^{13}C$ and $\delta^{15}N$ in CRMs were considered $< 0.3‰$, which confirms the accuracy of isotopic analysis. To eliminate the $\delta^{13}C$ fractionation effect associated with the lipid formation in fish, a mathematical lipid correction based on the C:N molar ratio was used and calculated as $\delta^{13}C_{corr}$ (Hoffman et al., 2015; Lepak et al., 2022). The C:N molar ratios of all the samples are listed in Table S2.

In addition, we estimated the TL for each fish sample using the corresponding $\delta^{15}N$ values and baseline $\delta^{15}N$ values. The TL of each sample was calculated using Eq. (1) (Xu et al., 2016):

$$TL = 1 + \left(\delta^{15}N_{sample} - \delta^{15}N_{baseline}\right)/3.4‰ \quad (1)$$

where $\delta^{15}N_{sample}$ represents the $\delta^{15}N$ values of the samples as reported in our previous study (Yang et al., 2022). The $\delta^{15}N_{baseline}$ corresponds to the $\delta^{15}N$ values in producers of the different regions. We measured the $\delta^{15}N$ values of phytoplankton collected from the estuary, MCS, and pelagic zone of SCS to estimate the baseline $\delta^{15}N$ values (5.44‰, 4.46‰, and 2.54‰ in the estuary, MCS, and pelagic zone, respectively) in different regions (Hong et al., 2013).

2.4. Hg isotope analysis

Hg isotopes in the samples were measured using a Nu-Plasma II multi-collector inductively coupled plasma mass spectrometer (MC-ICP-MS) at the State Key Laboratory of Environmental Geochemistry, Institute of Geochemistry, Chinese Academy of Sciences. The Hg isotopes in the seawater samples were analysed using the method proposed by Li et al. (2019). Initially, 10 L of the collected samples was oxidized with 0.1% BrCl solution for at least 48 h to allow the Hg species in the samples to be converted to Hg^{2+}. Thereafter we added 0.5% $SnCl_2$ to reduce Hg^{2+} to Hg^0, and it was purged with 2.5 L/min of zero-Hg gas for 1 h to transfer the evaporated Hg into a chlorinated activated carbon tube. Finally, the Hg in chlorinated activated carbon tube was removed by a pyrolysis device and absorbed into 5 mL of 40% anti-aqua regia, and stored at 4 °C and kept in the dark prior to Hg isotope analysis (Li et al., 2019). The National Institute of Standards and Technology Standard Reference Materials 3133 (NIST SRM 3133) was added to deionised water to be used as a CRM ($n = 3$) for seawater Hg isotope analysis (Yan et al., 2023). For fish samples, about 0.2 g of fish tissue was digested in 5 mL of HNO_3 at 95 °C for 3 h, and 0.5 mL of BrCl (30%) was subsequently added into the digested solution to maintain Hg stability. The Hg^{2+} digested solution was diluted using deionised water to approximate an acidity percentage of 20% and 1 $ng{\cdot}g^{-1}$ of Hg concentration before the Hg isotope measurement. TORT 3 (lobster, $n = 3$), and BCR 482 (lichen, $n = 3$) were used as CRMs to estimate the pre-treatment uncertainties of Hg isotopes in the fish samples. Hg isotope solutions of seawater and fish were introduced into the MC-ICP-MS by continuously reducing Hg^{2+} with 3% $SnCl_2$ and separating Hg^0 using a glass gas-liquid phase separator. The CRMs of NIST SRM 3177 ($n = 3$) and NIST RM 8610 ($n = 6$) were used to estimate the analytical uncertainties. Table S3 summarizes $\delta^{202}Hg$, $\Delta^{199}Hg$, $\Delta^{200}Hg$, and $\Delta^{201}Hg$ values of NIST SRM 3177, NIST

RM 8610, TORT 3, and BCR 482 measured in this study and those reported by other laboratories. According to the isotopic analysis precision of the MC-ICP-MS, the standard deviation (SD) for δ^{202}Hg, Δ^{199}Hg, Δ^{200}Hg, and Δ^{201}Hg were 0.10‰, 0.04‰, 0.04‰ and 0.04‰, respectively.

2.5. Hg isotope binary mixing model

A binary mixing model was used to evaluate the quantitative contribution of MeHg bioaccumulation from various environmental end-member sources using the following equations:

$$\Delta^{200}Hg_{fish} = \Delta^{200}Hg_{f1} \times f1 + \Delta^{200}Hg_{f2} \times f2 \quad (2)$$

$$f1 + f2 = 1 \quad (3)$$

where *f1* and *f2* represent the expected contribution of MeHg derived from each source based on the observed Δ^{200}Hg in marine fish. The environmental end-member sources depend on where the fish were collected from, as described in the Discussion section. The SD values of the calculated contributions were estimated using a Monte Carlo error propagation approach ($n = 10{,}000$) using the Python 3.9 software (Yang et al., 2021).

2.6. Data analysis

Correlations between measured variables were characterized using linear regression analysis, and the statistical significance of the correlation was evaluated using SPSS 19.0 and Origin 2021 statistical software for Windows. In addition, the York regression was used for Δ^{199}Hg/Δ^{201}Hg slopes in this work (York et al., 2004). The THg concentration, MeHg concentration, δ^{13}C, δ^{15}N, and Hg isotope values of all samples were compared using a non-parameter test (Mann–Whitney test) at the 5% significance level.

3. Results and discussion

3.1. THg and MEhG concentrations and Hg isotope composition in seawater

Fig. 2a shows the THg and MeHg concentrations in the seawater samples. Further information on the THg and MeHg concentrations and MeHg/THg ratios (%) for each seawater samples is given in Table S4. Overall, the mean concentrations (± 1SD) of THg in seawater were 5.52 ± 4.96 ng·L^{-1} (1.22–24.4 ng·L^{-1}), 2.40 ± 0.745 ng·L^{-1} (1.88–2.93 ng·L^{-1}), and 1.27 ± 0.399 ng·L^{-1} (0.77–1.70 ng·L^{-1}) in the estuary,

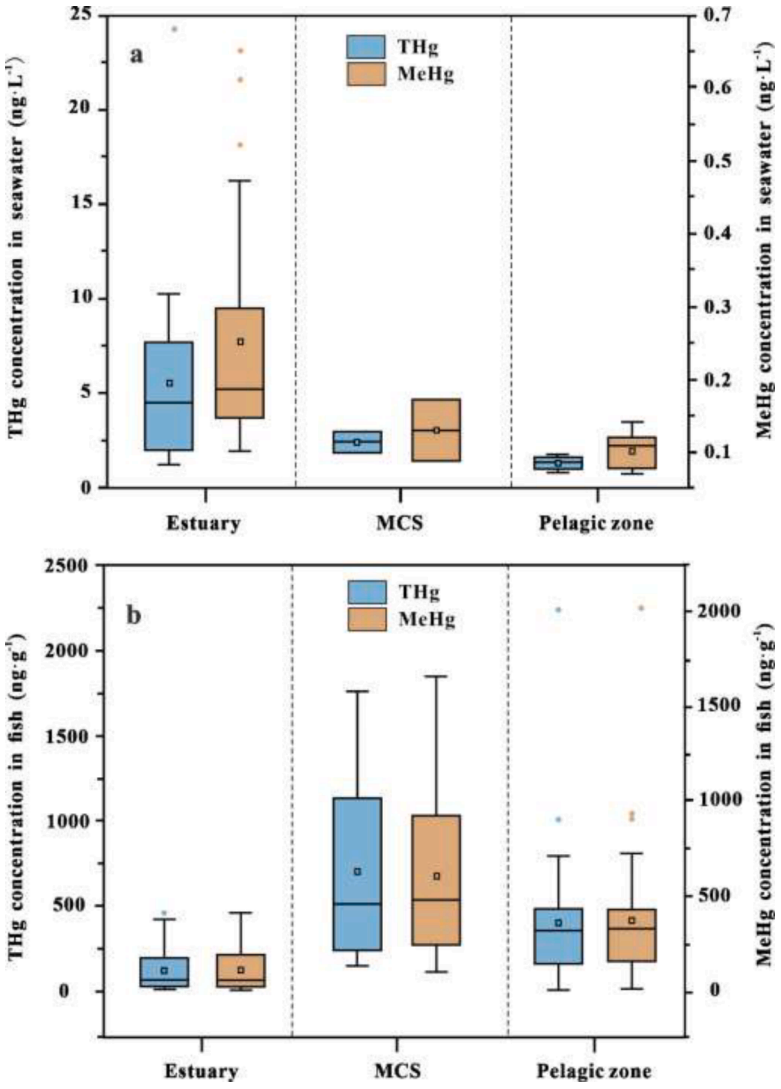

Fig. 2. (a) Box-plot of total Hg (THg) concentration and methylmercury (MeHg) concentration in seawater collected from the estuary, marine continental shelf (MCS), and pelagic zone of the South China Sea (SCS). Solid symbols represent outlier values. (b) Box-plot of THg and MeHg concentrations in marine fish collected from the estuary, marine continental shelf (MCS), and pelagic zone of the South China Sea (SCS). Solid symbols represent outlier values.

MCS, and pelagic zone, respectively (Fig. 2a). The differences in THg concentrations in seawater from the evaluated marine compartments were statistically significant ($p < 0.05$). MeHg in seawater showed comparable contents between the pelagic zone and MCS ($p > 0.05$), which were 0.130 ± 0.0566 ng·L^{-1} (0.0900−0.170 ng·L^{-1}) and 0.104 ± 0.0288 ng·L^{-1} (0.0700−0.140 ng·L^{-1}), respectively. However, estuarine seawater exhibited significantly higher ($p < 0.05$) MeHg values, with an average of 0.251 ± 0.160 ng·L^{-1} (0.100−0.650 ng·L^{-1}) (Fig. 2a). The average MeHg/THg ratios of seawater were 6.57% ± 4.16%, 6.07% ± 4.24% and 8.80% ± 2.99% in the estuary, MCS and pelagic zone, respectively (Table S4), which were similar to previous observations stating that the MeHg/THg ratio in seawater is generally lower than 10% (Fu et al., 2010; Lamborg et al., 2008; Wang et al., 2020). The THg and MeHg concentration in MCS and pelagic seawater of this study were similar to those reported in background coastal sea environments, such as those in the Northern SCS (THg: 0.8 − 2.3 ng·L^{-1}, MeHg: 0.05−0.22 ng·L^{-1}), Bohai Sea and Yellow Sea (THg: 0.75−3.94 ng·L^{-1}, MeHg: 0.05−0.22 ng·L^{-1}) and in the Coast of Black Sea (THg: 0.32−2.0 ng·L^{-1}, MeHg: 0.01−0.2 ng·L^{-1}) (Fu et al., 2010; Lamborg et al., 2008; Wang et al., 2020). However, the THg concentration in estuarine seawater were nearly 4-folds higher than that in pelagic and MCS seawater, and 2-folds for MeHg in the same environments (Fig. 2a). Especially, anomalous high concentrations of THg (> 10 ng·L^{-1}) were found in the sampling sites of PRE-S3 (10.2 ng·L^{-1}), PRE-S6 (24.4 ng·L^{-1}), PRE-S7 (10.2 ng·L^{-1}) (Fig. 2a; Table S4), which suggested the potentially anthropogenic Hg input to estuarine seawater. Therefore, Hg isotope compositions were further analysed to compare the differences in Hg sources for the seawater collected from the three marine compartments.

The mean values of δ^{202}Hg, Δ^{199}Hg, Δ^{200}Hg, and Δ^{201}Hg measured in the SCS seawater are presented in Table 1, and detailed information on the Hg isotope compositions of each seawater sample is given in Table S5. In general, δ^{202}Hg in all of seawater samples showed negative values and varied widely range (from −2.23‰ to −0.50‰); this result resembled previous observations conducted in Chinese coastal seawater (Fig. 3a), such as Guangxi and Fujian coastal mangrove (from −1.39‰ to −0.94‰, $n = 14$), Yundang Lagoon (from −2.18‰ to −1.06‰, $n = 7$), and Bohai Sea (from −1.28‰ to −1.14‰, $n = 2$) (Huang et al., 2020, 2021; Meng et al., 2020). Besides, such values were slightly higher than those in terrestrial runoff, such as those in the northern Sweden forest runoff (from −2.29‰ to −1.76‰, $n = 7$) and in the northern Minnesota forest stream (from −2.12‰ to −1.32‰, $n = 24$) (Jiskra et al., 2017; Woerndle et al., 2018). In contrast, Δ^{199}Hg (from 0.01‰ to 0.21‰), Δ^{200}Hg (from 0.05‰ to 0.08‰) and Δ^{201}Hg (from −0.07‰ to 0.09‰) spanned a relatively narrow range (Table S5). Seawater collected from the three marine compartments showed comparable values ($p > 0.05$) of Δ^{199}Hg (estuary: 0.09‰ ± 0.10‰; MCS: 0.10‰ ± 0.14‰; pelagic zone: 0.04‰ ± 0.03‰), Δ^{200}Hg (estuary: −0.01‰ ± 0.06‰; MCS: 0.01‰ ± 0.03‰; pelagic zone: −0.01‰ ± 0.05‰) and Δ^{201}Hg (estuary: 0.03‰ ± 0.07‰; MCS: 0.03‰ ± 0.04‰; pelagic zone: 0.01‰ ± 0.03‰) (Table 1). Similar Δ^{199}Hg, Δ^{200}Hg and Δ^{201}Hg values in seawater from different compartments lead to complications in distinguishing Hg sources (Fig. 3a). However, significant differences in δ^{202}Hg values were found between estuarine and pelagic seawater. δ^{202}Hg in seawater of the estuary (from −2.23‰ to −1.30‰, −1.63‰ ± 0.42‰) was significantly lower ($p < 0.05$) than that in the pelagic zone (from −0.65‰ to −0.50‰, −0.58‰ ± 0.08‰); whereas MCS seawater presented similar δ^{202}Hg values (from −1.16‰ to −0.72‰, −0.94‰ ± 0.31‰), compared with those in estuarine and pelagic zone seawater ($p > 0.05$) (Table 1). In addition, a significant negative correlation was found between the THg concentration and δ^{202}Hg in all seawater samples (Fig. 3b), suggesting distinct sources of Hg in the three marine compartments. δ^{202}Hg values of the pelagic seawater are in the range of Mediterranean and North Atlantic seawater (from −1.18‰ to 0.10‰, $n = 16$) (Jiskra et al., 2021). In the pelagic ocean, atmospheric deposition (dry and wet deposition) represented the predominant pathway of Hg input into the seawater; moreover, it has been reported that gas elemental Hg (GEM) and precipitation samples contain δ^{202}Hg values proximate to 0‰ (Jiskra et al., 2021; Tsui et al., 2020b). The relatively high value of δ^{202}Hg in pelagic seawater observed in this study may be explained by atmospheric Hg deposition. However, terrestrial Hg (forest litter, organic soil and mineral soil) tend to present negative δ^{202}Hg value (Tsui et al., 2020b; Woerndle et al., 2018); for instance, organic soil (located at the surface layer of soil) generally exhibits a δ^{202}Hg value lower than −1.5‰ (Demers et al., 2013; Kwon et al., 2020; Smith et al., 2008). Studies conducted in freshwater environments have demonstrated that Hg bound to organic matter represents a large fraction of Hg in runoff (Jiskra et al., 2017). Watershed inputs can erode and transport terrestrial Hg into estuarine area, leading to relatively low δ^{202}Hg values in estuarine seawater. Furthermore, seawater in PRE-S7 showed high concentration of THg (10.2 ng·L^{-1}) and the highest negative value of δ^{202}Hg (−2.23‰). Rapid economic development and population increases have aggravated human discharge of Hg around the estuarine areas of the SCS (Yang et al., 2022; Yu et al., 2010). Previous observations have demonstrated that industrial sources of Hg often present δ^{202}Hg values between 1‰ and 0‰ (Balogh et al., 2015; Emslie et al., 2015), which suggests that high Hg concentration in PRE-S7 was unaffected by industrial Hg pollution. In contrast, Zhang et al. (2020) reported that domestic wastewater has markedly negative δ^{202}Hg values (−2.48‰ ± 0.10‰) compared to other kinds of sewage and terrestrial water input in PRE, and which is consistent with δ^{202}Hg in PRE-S7. Therefore, the Hg isotope results showed that, in addition to watershed input, domestic wastewater may also act as an important Hg source in estuarine areas with rapid population growth. We propose that different sources of Hg can, to a large extent, cause the Hg in the estuarine and pelagic zone to exhibit distinct δ^{202}Hg values. δ^{202}Hg values of the MCS may be explained by the mixing of estuarine and pelagic Hg.

Table 1
Hg isotope compositions (δ^{202}Hg, Δ^{199}Hg, Δ^{200}Hg and Δ^{201}Hg) in seawater and marine fish collected from different compartments (estuary, marine continental shelf (MCS), and pelagic zone) of the South China Sea.

Samples	n	δ^{202}Hg (‰)	Δ^{199}Hg (‰)	Δ^{200}Hg (‰)	Δ^{201}Hg (‰)
Fish samples					
Estuary	31	−0.07 ±0.27	0.39±0.35	0.07±0.02	0.41±0.30
MCS	24	−0.20 ±0.24	1.10±0.54	0.05±0.06	0.83±0.46
Pelagic zone	34	0.53±0.32	1.15±0.46	0.10±0.04	0.94±0.37
Seawater samples					
Estuary	4	−1.63 ±0.42	0.09±0.10	−0.01 ±0.06	0.03±0.07
MCS	2	−0.94 ±0.31	0.10±0.14	0.01±0.03	0.03±0.04
Pelagic zone	3	−0.58 ±0.08	0.04±0.03	−0.01 ±0.05	0.01±0.03

3.2. Hg levels and C and N isotope properties in marine fish

The THg concentrations in marine fish samples have been reported in our previous work (Yang et al., 2022) and are presented in Fig. 2b. Although pelagic fish showed significantly lower TL compared to MCS and estuarine fish (Table S6), we found that fish collected from MCS exhibited the highest THg concentration (742 ± 520 ng·g^{-1}), followed by those from the pelagic zone (451 ± 378 ng·g^{-1}), and the lowest THg concentration was found in estuarine fish (143 ± 127 ng·g^{-1}) (Fig. 2b). Similarly, large variations in MeHg concentrations (11.3 − 2040 μg/kg) were found in all fish samples (Table S6). Fish from the different compartments exhibited significantly different MeHg contents ($p < 0.05$), with concentrations in MCS (131−1690 ng·g^{-1}; 635 ± 464 ng·g^{-1}) > pelagic zone (31.5 − 2040 ng·g^{-1}; 403 ± 362 ng·g^{-1}) > estuary (11.3 −

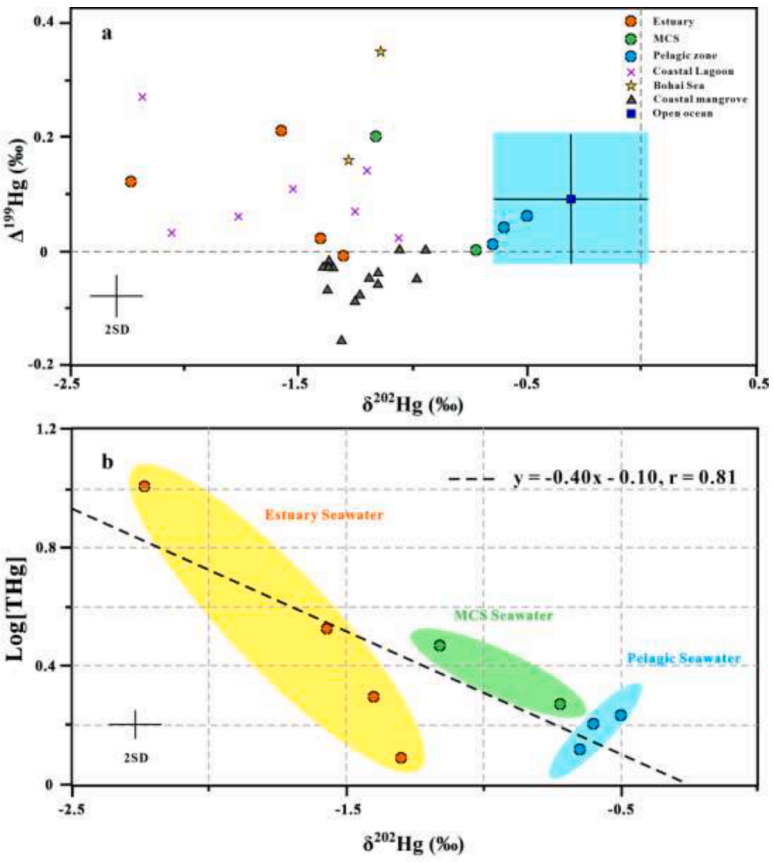

Fig. 3. (a) δ^{202}Hg and Δ^{199}Hg values measured in seawater samples collected from the estuary, marine continental shelf (MCS), and pelagic zone of the South China Sea (SCS) (present study), Guangxi and Fujian coastal mangroves (Huang et al., 2020), Yundang Lagoon (Huang et al., 2021), Bohai Sea (Meng et al., 2020), and the open ocean (Jiskra et al., 2021). (b) Linear regressions between δ^{202}Hg value and the logarithmic value of total Hg concentration (log[THg]). The orange, green, and blue spots represent seawater samples collected from the estuary, marine continental shelf (MCS), and pelagic zones of the South China Sea (SCS), respectively.

421 ng·g^{-1}; 116 ± 119 ng·g^{-1}) (Fig. 2b). The average MeHg/THg ratios of marine fish were 75.1% ± 17.1%, 85.6% ± 10.0% and 86.5% ± 9.57% in the estuary, MCS, and pelagic zone, respectively (Table S6). Details of the THg and MeHg concentrations and the MeHg/THg ratios (%) in the marine fish samples are given in Table S6. Although high THg and MeHg concentrations were found in estuarine seawater, the Hg concentration in fish from the estuarine region was relatively low (Fig. 2b). This low value may be explained by the increased demand for fish driven by rapid population growth in the PRE region, which has resulted in a series of ecological modification effects, such as food chain length shortage and Hg biomagnification suppression (Tsui et al., 2022).

The $\delta^{13}C_{corr}$ and $\delta^{15}N$ values for all fish samples are presented in Fig. S1. Other details of the $\delta^{13}C_{corr}$, $\delta^{15}N$, and TL values for each marine fish sample are provided in Table S6. $\delta^{13}C_{corr}$ value in fish varied from −23.3‰ to −11.6‰, with significantly different values ($p < 0.05$) were observed in the fish of the three compartments, i.e., pelagic zone (from −18.7‰ to −11.6‰, −15.3‰ ± 1.30‰) > MCS (from −21.3‰ to −12.0‰, −16.5‰ ± 2.40‰) > estuary (from −23.3‰ to −15.6‰, −19.5‰ ± 2.07‰) (Fig. S1a). Given the conservation of $\delta^{13}C$ enrichment/depletion (< 0.4‰) during trophic transfer, $\delta^{13}C$ measurement is a useful approach for identifying the dietary sources of aquatic species (Xu et al., 2016). Marine fish have been previously shown to possess higher $\delta^{13}C$ values (−21.3‰ to −14.4‰) than those of freshwater fish (−29.4‰ to −24.5‰) (Asante et al., 2008, 2010; Gu et al., 2018; Wang et al., 2011); this could be explained by the different $\delta^{13}C$ signals exhibited by the primary organic matter in marine (−21.0‰ to −18.0‰) and terrestrial (−27.0‰ to −25.0‰) ecosystems (Fry, 1988; Peterson and Fry, 1987). Relatively negative $\delta^{13}C_{corr}$ values in estuarine fish may indicate terrestrial dietary sources, whereas significantly less negative $\delta^{13}C_{corr}$ values in pelagic fish may suggest marine dietary sources. $\delta^{13}C_{corr}$ characteristics of the MCS are likely attributable to the mixing of estuarine and pelagic diets (Fig. S1a). $\delta^{15}N$ values were reported in our previous studies (Yang et al., 2022). $\delta^{15}N$ values in fish of pelagic zone (7.01‰–9.55‰, 8.47‰ ± 0.562‰) were significantly lower ($p < 0.01$) than those in MCS (7.42‰–15.3‰, 11.8‰ ± 2.09‰) and in the estuary (9.10‰–16.6‰, 12.8‰ ± 1.57‰), whereas those of MCS and estuarine fish were comparable ($p > 0.05$) (Fig. S1b). Both trophic transfer enrichment and the food web baseline values of $\delta^{15}N$ can affect the $\delta^{15}N$ ratios in marine fish (Perrot et al., 2019; Senn et al., 2010; Xu et al., 2016). $\delta^{15}N$ baseline in ecosystems can be represented by bulk $\delta^{15}N$ in phytoplankton. Differences in $\delta^{15}N$ values (Section 2.3) amongst estuarine, MCS and pelagic phytoplankton suggested distinct N input amongst the three marine compartments. The overall TL of the collected fish ranged from 1.87 to 4.28, and the values of TL in MCS (TL = 3.16 ± 0.615) and estuary (TL = 3.17 ± 0.469) fish were comparable ($p > 0.05$) and both were higher than those in pelagic fish (TL = 2.74 ± 0.165) ($p < 0.01$) (Table S6).

Hg levels, C and N isotopes showed distinct patterns in the marine fish collected from the three marine compartments. $\delta^{13}C_{corr}$ and $\delta^{15}N$ in all samples showed a significantly negative linear regression (Fig. S2); however, no correlation was observed between $\delta^{13}C_{corr}$ and $\delta^{15}N$ at each site, indicating that C and N isotopes could be used to differentiate amongst fish from diverse geographical regions in marine ecosystems. Furthermore, although Hg levels, dietary sources, and food web structures were different, we found that TL and log[MeHg] were positively correlated in all regions (Fig. S3), suggesting that biomagnification plays an important role in determining MeHg concentration in marine fish.

3.3. *Hg isotope composition and underlying processes of MeHg in marine fish*

The mean values of δ^{202}Hg, Δ^{199}Hg, Δ^{200}Hg and Δ^{201}Hg measured in the fish of this study are shown in Table 1. A comparison of δ^{202}Hg and Δ^{199}Hg in the fish and seawater samples is shown in Fig. 4a. Fish

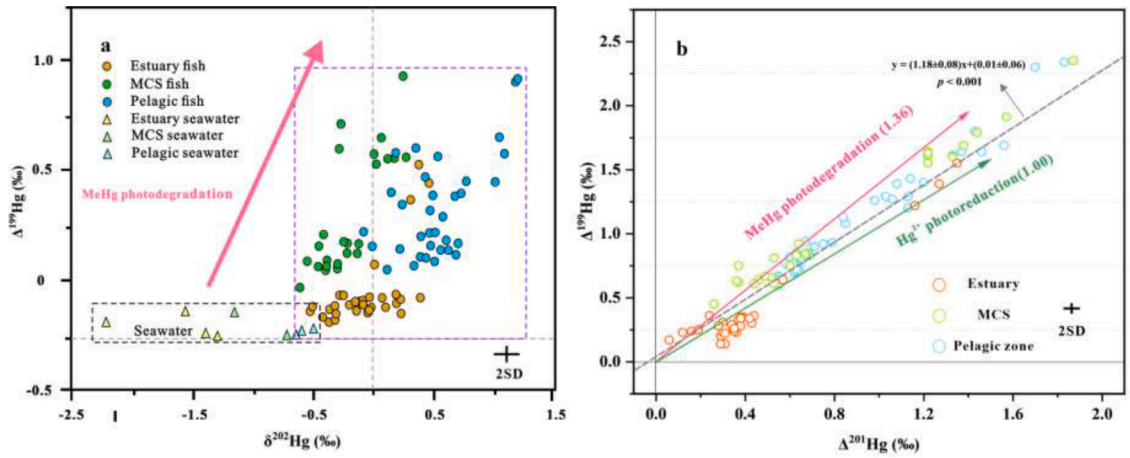

Fig. 4. (a) δ^{202}Hg and Δ^{199}Hg values measured in seawater and marine fish collected from the estuary, marine continental shelf (MCS), and pelagic zone of the South China Sea (SCS). The pink arrow represents the slope of MeHg photodegradation (slope = 2.43). (b) York regressions between two odd mass-independent fractionation characteristics (Δ^{199}Hg vs. Δ^{201}Hg). The orange, green, and blue spots represent fish collected from the estuary, marine continental shelf (MCS), and pelagic zones of the South China Sea (SCS), respectively. The pink arrow represents the slope of MeHg photodegradation (slope = 1.36 ± 0.04), and the green arrow represents the slope of Hg(II) reduction (slope = 1.00 ± 0.02).

samples presented a wide range of δ^{202}Hg (from −0.61‰ to 1.23‰), Δ^{199}Hg (from 0.14‰ to 2.35‰), and Δ^{201}Hg (from 0.06‰ to 1.87‰); whereas they showed a relatively narrow range of Δ^{200}Hg (from −0.07‰ to 0.18‰) (Table S5). δ^{202}Hg in fish of the estuary (from −0.53‰ to 0.46‰, −0.07‰ ± 0.27‰) and MCS (from −0.61‰ to 0.28‰, −0.20‰ ± 0.24‰) were comparable ($p > 0.05$); however, significantly heavier ($p < 0.01$) δ^{202}Hg were found in pelagic fish (from −0.01‰ to 1.23‰, 0.53‰ ± 0.32‰) (Table 1; Table S5). The mean value of δ^{202}Hg in MCS and estuarine fish were both close to 0, which is similar to those of organisms collected in the PRE area (0.14‰ ± 0.20‰, $n = 18$) and the East coast of China (−0.07‰ ± 0.50‰, $n = 27$) (Yang et al., 2021; Yin et al., 2016). However, the δ^{202}Hg values in pelagic fish were proximate to that in the North Pacific Ocean (NPO, 0.63‰ ± 0.42‰, $n = 28$) (Blum et al., 2013). Δ^{199}Hg values were similar for both pelagic (0.60‰−2.34‰, 1.15‰ ± 0.46‰) and MCS (0.45‰−2.35‰, 1.10‰ ± 0.54‰) fish ($p > 0.05$), which are significantly higher ($p < 0.01$) than that in estuarine fish (0.14‰−1.55‰, 0.39‰ ± 0.35‰) (Table 1; Table S5). Similarly, the results of Δ^{201}Hg closely corresponded with the Δ^{199}Hg measurements, which ranged from 0.06‰ to 1.35‰ (0.41‰ ± 0.30‰), 0.26‰ to 1.87‰ (0.83‰ ± 0.46‰), and 0.55‰ to 1.83‰ (0.94‰ ± 0.37‰) for estuarine, MCS, and pelagic fish, respectively (Table 1; Table S5). Finally, Δ^{200}Hg values showed comparable patterns ($p > 0.05$) in fish of MCS (−0.07‰−0.16‰, 0.05‰ ± 0.06‰) and estuary (0.02‰−0.11‰, 0.07‰ ± 0.02‰); whereas fish of pelagic zone had significantly higher ($p < 0.01$) Δ^{200}Hg values (0.02‰−0.18‰, 0.10‰ ± 0.04‰), compared with those in the estuary and MCS (Table 1; Table S5). Details of the Hg isotope compositions of each fish sample are provided in Table S5.

Odd-MIF occurs alongside with MeHg photodegradation and Hg(II) photoreduction in aquatic ecosystems (Bergquist and Blum, 2007). Given the absence of photochemical reactions during trophic transfer processes, Δ^{199}Hg and Δ^{201}Hg values in organisms reflect the odd-MIF composition of MeHg prior to its entering the food web (Tsui et al., 2020a). Moreover, the Δ^{199}Hg/Δ^{201}Hg ratio is a diagnostic method to identify the two photochemical reaction types, with an experimental value of ~1.36 for MeHg photodegradation and ~1.0 for Hg(II) photoreduction (Blum et al., 2014). Δ^{199}Hg and Δ^{201}Hg values in all fish samples were positively correlated (with a slope of 1.18 ± 0.01 (York Regression), Fig. 4b), which is consistent with previous work conducted in coastal areas (e.g., PRE area [slope = 1.26] and the East coast of China [slope = 1.22]) (Yang et al., 2021; Yin et al., 2016). This result suggested that the odd-MIF in fish of this work is produced by MeHg photodegradation processes. In contrast, Hg isotopes detected in seawater generally indicate the IHg behaviour because of the high percentage of IHg in seawater. Relatively higher δ^{202}Hg and Δ^{199}Hg values in MeHg compared with those in IHg were mainly attributed to the MeHg photodegradation (Fig. 4a).

In this study, notably smaller Δ^{199}Hg and Δ^{201}Hg values were observed in the estuarine fish than those in the Great Lakes, open ocean, plateau lakes, and most of coastal bays (except the Bohai Bay). Conversely, MCS and pelagic fish exhibited relatively higher odd-MIF, which were only lower than those of the open ocean and Great Lakes (Fig. S4). All fish considered in the present study had a habitat depth of < 200 m, which reduced the vertical Hg isotope variation in the ocean (Blum et al., 2013). Therefore, we propose that much less MeHg photodegradation occurred in estuarine seawater than in the MCS and pelagic seawater. The extent of MeHg photodegradation is affected by light intensity and dissolved organic carbon (DOC) levels (Bergquist and Blum, 2007; Lepak et al., 2018). Earlier findings demonstrated that the DOC concentration in the PRE region and in the northern slope of SCS were comparable (approximately 1.33 mg/L and 0.91 mg/L, respectively) (He et al., 2010; Zhang et al., 2019). However, the water turbidity of the PRE seawater (4.5 NTU) is significantly higher than that in the open ocean of the SCS (1 NTU) (Wang et al., 2021). Thus, the low extent of MeHg photodegradation in the estuarine region of the SCS can be explained by the high turbidity of seawater, which directly reduces the light intensity. We quantified the percentage of MeHg photodegradation based on Δ^{199}Hg using a previously reported method (Bergquist and Blum, 2007), which was expected to help elucidate the differences in the potential photochemical processes of MeHg in the estuary, MCS, and pelagic zones of the SCS. We estimated that 12% ± 9%, 31% ± 13%, and 33% ± 11% of MeHg occurred photodegradation prior to entering the food web in the estuary, MCS, and pelagic zones of SCS, respectively. Except for external Hg input, relatively weak MeHg photodegradation may act as another factor to explain high MeHg concentration in seawater of the estuarine region.

3.4. Primary sources of mehg in marine fish

It has been reported that most biogeochemical processes do not cause even-MIF except for the atmospheric photooxidation process, which can lead to positive Δ^{200}Hg in precipitation (Chen et al., 2012). Thus, Δ^{200}Hg can be used as a proxy to investigate MeHg sources related to atmospheric deposition in the environment (Jiskra et al., 2021). A comparison of Δ^{200}Hg values of estuary, MCS, and pelagic fish from the SCS (this study), Bohai Bay (BHB) (Meng et al., 2020), NPO (Blum et al.,

2013), the East Pacific Ocean (Madigan et al., 2018), and the Great Lakes (Lepak et al., 2018) is shown in Fig. 5. Previous works have found that fish collected from open ocean generally show positive Δ^{200}Hg (He et al., 2023), which is consistent with the data found in pelagic fish. The pelagic region of the SCS (with a depth > 1000 m) is barely affected by any external Hg sources, such as watershed, and sediment disturbances. In addition, the presence of coral reefs indicate that no frequent volcanic activity in the SCS since the early Pleistocene (Zhan et al., 2006), which excludes geological Hg input to the pelagic zone of the SCS. Therefore, the pelagic zone can be considered to have absorbed Hg from the atmosphere. Atmospheric Hg can enter marine ecosystems through wet and dry Hg(II) deposition as well as Hg(0) dissolution (Blum et al., 2013; Kwon et al., 2020). Hg(II) is associated with cloud droplets and is concentrated in precipitation, causing rainfall samples to have a positive Δ^{200}Hg. Recent models suggest that in ocean regions, the combination of wet and dry Hg(II) deposition maintain the Δ^{200}Hg values between 0.11‰ and 0.20‰ around the latitude of 15° N; meanwhile, Hg(0) showed an average Δ^{200}Hg value of −0.06‰ (median, interquartile range: −0.08‰ to −0.02‰) (Demers et al., 2015; Fu et al., 2018; Jiskra et al., 2021). Significant differences in Δ^{200}Hg values were observed between Hg(II) and Hg(0) end-members ($p < 0.001$). Thus, the isotopic mixing binary model, explained in Section 2.5, can quantify the atmospheric contribution of Hg(II) and Hg(0) in fish in the pelagic zone.

The results showed that atmospheric Hg(II) contributes 74% ± 11% (1SD) of MeHg to pelagic fish. Recent studies proposed that Hg methylation in seawater generally occurs in the water column at the oxygen minimum zone (OMZ) (Krabbenhoft and Sunderland, 2013; Blum et al., 2013). Hg(II) can be transported from the ocean surface to the OMZ by binding to sinking particles, which are finally methylated to MeHg (Lepak et al., 2018; Motta et al., 2022; Sun et al., 2020). Subsequently, MeHg migrates to the upper ocean through upwelling and is absorbed by various algae and bacteria, which finally accumulate in marine fish (Blum et al., 2013). Considering the absence of even-MIF during Hg methylation, upwelling transportation and MeHg biomagnification, MeHg formed in marine fish tends to retain the Δ^{200}Hg characteristics of Hg(II). Conversely, Hg(0) in seawater has not been found to be directly involved in the Hg methylation processes (Blum et al., 2013). As a result, the water column exhibits high lability and susceptibility to the methylation of Hg(II), leading to increased bioaccumulation of MeHg in marine fish from atmospheric Hg(II) sources.

In addition, as the MCS region is far from mainland of China and is weakly affected by riverine input (Fig. 1), we propose that sedimentary and atmospheric inputs are the two predominant sources of MeHg accumulated in fish. The atmospheric Hg input is mainly related to precipitation, which is linked to latitude (Chen et al., 2012; Jiskra et al., 2021). Thus, the comparable latitudes of the MCS and pelagic zones of the SCS should yield similar Δ^{200}Hg values for local fish (Fig. 1). Because pelagic fish possessed significantly higher values of Δ^{200}Hg than SCS coastal sediment ($p = 0.006$), the significantly lower Δ^{200}Hg values in MCS fish may be attributable to the contribution of sediment Hg. Again, using the Hg isotope binary mixing model, we estimated the contribution of sedimentary Hg to MCS fish (Section 2.5). The two end members were atmospheric Hg and sedimentary Hg. The Δ^{200}Hg values for atmospheric Hg were considered equal to those for pelagic fish (mean: 0.10‰; interquartile range: 0.09‰–0.11‰), and the Δ^{200}Hg values for sediment (mean: 0.01‰; interquartile range: 0.00‰–0.02‰) were provided by Yin et al. (2015). The results showed that sediment contributed 62% ± 19% of the bioaccumulated MeHg in MCS fish, which is an important observation for the development of marine Hg food web models. Overall, Δ^{200}Hg values in marine fish can provide information on atmospheric Hg deposition, particularly for understanding the contribution of Hg(II) and Hg(0) to MeHg bioaccumulation. However, because of the small variation in Δ^{200}Hg in the environment, the Δ^{200}Hg binary mixing model has limitations to some extent. For instance, distinguishing end-member and calculating uncertainties need to be achieved carefully. Further studies are required to develop highly precise Hg measurement methods to enhance the application of Δ^{200}Hg.

Finally, MeHg accumulated in estuarine fish may be obtained from riverine inputs, anthropogenic emissions (Section 3.1), sediment release and atmospheric deposition, which represent a complex ecosystem (Bosignore et al., 2015; Yin et al., 2015, 2016). Riverine Hg input can elevate Δ^{200}Hg values in estuarine fish, which is consistent with relatively higher Δ^{200}Hg signatures determined in watershed rivers in the estuarine zones of SCS in a previous work (mean: 0.08‰; interquartile range: 0.04‰–0.09‰) (Zhang et al., 2020). However, in the application of the Δ^{200}Hg mixing model, separating several endmembers is difficult; therefore, we did not quantify the MeHg sources in estuarine fish. Advanced approaches (e.g. MeHg-specific isotope analysis) need to be developed to quantify MeHg sources in estuarine fish and to establish comprehensive profiles for Hg biogeochemical cycling in the marine ecosystems.

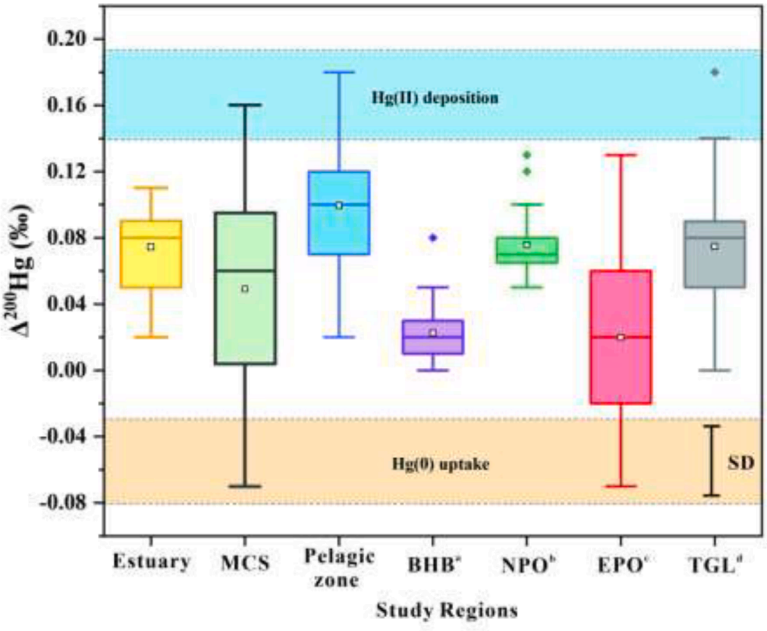

Fig. 5. Δ^{200}Hg values in fish collected from the estuary, marine continental shelf (MCS), and pelagic zones of the South China Sea (SCS) (present study); Bohai Bay (BHB, Liu et al., 2018); North Pacific Ocean (NPO, Blum et al., 2013); East Pacific Ocean (EPO, Madigan et al., 2018); and the Great Lakes (TGL, Lepak et al., 2018). Δ^{200}Hg in atmospheric deposition sources are depicted by horizontal bars (interquartile range) in brown for Hg(0) and blue for Hg(II) (Demers et al., 2015; Fu et al., 2018; Jiskra et al., 2021).

4. Conclusion

Hg isotopes were used to identify the sources and processes of Hg in food webs within three differing marine compartments (e.g. estuary, MCS and pelagic zone). The estuarine seawater had significantly higher THg and MeHg levels than the MCS and pelagic seawater. Compared with the pelagic zone, estuarine seawater had a lower δ^{202}Hg value, suggesting Hg sources from watershed input and human sewage discharge. The combination of C—N isotopes can contributed to distinguishing the dietary sources and trophic levels of fish from the differing marine compartments. δ^{202}Hg, Δ^{199}Hg, and Δ^{201}Hg revealed the underlying processes of MeHg accumulation in fish collected from the estuary, MCS, and pelagic zone. Estuarine regions occurred notably low MeHg degradation due to its high water turbidity. In addition, Δ^{200}Hg value was used to quantify Hg sources in marine fish; distinct Δ^{200}Hg values in pelagic and coastal fish provide an overall profile of atmospheric Hg deposition, and helped us to understand contribution of Hg(II) and Hg(0). Moreover, the Δ^{200}Hg values presented information on the sedimentary Hg burden to MeHg bioaccumulation. Our observations support the idea that the analysis of Hg isotopes in seawater and fish provide comprehensive on the behaviour of Hg in marine ecosystems. However, quantifying Hg sources in estuarine fish remains challenging. Optimization of isotope mixing model parameters and MeHg-specific isotope analysis are essential to better understand the source portfolios using the Hg isotopic distribution in marine organisms.

Declaration of Competing Interest

The authors declare that they have no known competing financial interests or personal relationships that could have appeared to influence the work reported in this paper.

Data availability

Data will be made available on request.

Acknowledgements

This study was supported by the Fundamental Research Funds for the Central Universities, China University of Geosciences (Wuhan) (Nos. CUGCJ1703), the Central Public-Interest Scientific Institution Basal Research Fund (PM-zx097–202204–079), CAS Interdisciplinary Innovation Team (JCTD-2020–20) and the Youth Innovation Promotion Association, Chinese Academy of Sciences (Y2021106).

Supplementary materials

Supplementary material associated with this article can be found, in the online version, at doi:10.1016/j.watres.2023.120150.

References

Asante, K.A., Agusa, T., Kubota, R., Mochizuki, H., Ramu, K., Nishida, S., Ohta, S., Yeh, H., Subramanian, A., Tanabe, S., 2010. Trace elements and stable isotope ratios (δ^{13}C and δ^{15}N) in fish from deep-waters of the Sulu Sea and the Celebes Sea. Mar. Pollut. Bull. 60, 1560–1570.

Asante, K.A., Agusa, T., Mochizuki, H., Ramu, K., Inoue, S., Kubodera, T., Takahashi, S., Subramanian, A., Tanabe, S., 2008. Trace elements and stable isotopes (δ^{13}C and δ^{15}N) in shallow and deep-water organisms from the East China Sea. Environ. Pollut. 156, 862–873.

Balogh, S.J., Tsui, M.T., Blum, J.D., Matsuyama, A., Woerndle, G.E., Yano, S., Tada, A., 2015. Tracking the fate of mercury in the fish and bottom sediments of Minamata Bay, Japan, using stable mercury isotopes. Environ. Sci. Technol. 49, 5399–5406.

Bellanger, M., Pichery, C., Aerts, D., Berglund, M., Castano, A., Cejchanova, M., Crettaz, P., Davidson, F., Esteban, M., Fischer, M.E., Gurzau, A.E., Halzlova, K., Katsonouri, A., Knsdsen, L.E., Kolossa-Gehring, M., Koppen, G., Ligocka, D., Miklavcic, A., Reis, M.F., Rudnai, P.;., Tratnik, J.S., Weihe, P., Budtz-Jorgensen, E., Grandjean, P., DEMO/COPHES, 2013. Economic benefits of methylmercury exposure control in Europe: monetary value of neurotoxicity prevention. Environ. Health 12 (3).

Bergquist, B.A., Blum, J.D., 2007. Mass-dependent and -independent fractionation of Hg isotopes by photoreduction in aquatic systems. Science 318, 417–420.

Blum, J.D., Popp, B.N., Drazen, J.C., Choy, C.A., Johnson, M.W., 2013. Methylmercury production below the mixed layer in the North Pacific Ocean. Nat. Geosci. 6, 879–884.

Blum, J.D., Sherman, L., Johnson, M., 2014. Mercury isotopes in earth and environmental sciences. Annu. Rev. Earth Planet. Sci. 42, 249–269.

Bosignore, M., Tamburrino, S., Oliveri, E., Marchetti, A., Durante, C., Berni, A., Quinci, E., Sprovieri, M., 2015. Tracing mercury pathways in Augusta Bay (southern Italy) by total concentration and isotope determination. Environ. Pollut. 205, 178–185.

Chen, J., Hintelmann, H., Feng, X., Dimock, B., 2012. Unusual fractionation of both odd and even mercury isotopes in precipitation from Peterborough, ON, Canada. Geochim. Cosmochim. Acta 90, 33–46.

Croizier, G.L., Lorrain, A., Sonke, J.E., Jaquemet, S., Schaal, G., Renedo, M., Besnard, L., Cherel, Y., Point, D., 2020. Mercury isotopes as tracers of ecology and metabolism in two sympatric shark species. Environ. Pollut. 265, 114931.

Demers, J.D., Blum, J.D., Zak, D.R., 2013. Mercury isotopes in a forested ecosystem: implications for air-surface exchange dynamics and the global mercury cycle. Glob. Biogeochem. Cycles 27, 222–238.

Demers, J.D., Sherman, L.S., Blum, J.D., Marsik, F.J., Dvonch, J.T., 2015. Coupling atmospheric mercury isotope ratios and meteorology to identify sources of mercury impacting a coastal urban-industrial region near Pensacola, Florida, USA. Glob. Biogeochem. Cycles 29, 1689–1705.

Emslie, S.D., Brasso, R., Patterson, W.P., Valera, A.C., McKenzie, A., Silva, A.M., Gleason, J.D., Blum, J.D., 2015. Chronic mercury exposure in Late Neolithic/Chalcolithic populations in Portugal from the cultural use of cinnabar. Sci. Rep. 5, 14679.

Fry, B., 1988. Food web structure on Georges Bank from stable C, N, and S isotopic compositions. Limnol. Oceanogr. 33, 1182–1190.

Fu, X., Feng, X., Zhang, G., Xu, W., Li, X., Yao, H., Liang, P., Li, J., Sommar, J., Yin, R., Liu, N., 2010. Mercury in the marine boundary layer and seawater of the South China Sea: concentrations, sea/air flux, and implication for land outflow. J. Geophys. Res. Sol. Ea. 115, D06303.

Fu, X., Jiskra, M., Yang, X., Marusczak, N., Enrico, M., Chmeleff, J., Heimbürger-Boavida, L., Gheusi, F., Sonke, J.E., 2021. Mass-independent fractionation of even and odd mercury isotopes during atmospheric mercury redox reactions. Environ. Sci. Technol. 55, 10164–10174.

Fu, X., Yang, X., Tan, Q., Ming, L., Lin, T., Lin, C.J., Li, X., Feng, X., 2018. Isotopic composition of gaseous elemental mercury in the marine boundary layer of East China Sea. J. Geophys. Res. Atmos. 123, 7656–7669.

Gehrke, G.E., Blum, J.D., Slotton, D.G., Greenfield, B.K., 2011. Mercury isotopes link mercury in San Francisco Bay Forage fish to surface sediments. Environ. Sci. Technol. 45, 1264–1270.

Gu, Y.G., Ning, J.J., Ke, C.L., Huang, H.H., 2018. Bioaccessibility and human health implications of heavy metals in different trophic level marine organisms: a case study of the South China Sea. Ecotoxicol. Environ. Safe. 163, 551–557.

He, B., Dai, M., Zhai, W., Wang, L., Wang, K., Chen, J., Lin, J., Han, A., Xu, Y., 2010. Distribution, degradation and dynamics of dissolved organic carbon and its major compound classes in the Pearl River estuary, China. Mar. Chem. 119, 52–64.

He, X., Chen, Y., Ang, S., Shiao, J., Tseng, C., Reinfelder, J., 2023. Mercury stable isotopes reveal sources of methylmercury and prey in giant Pacific bluefin tuna from the western North Pacific Ocean. Limnol. Oceanogr. Lett. https://doi.org/10.1002/lol2.10313.

Hoffman, J.C., Sierszen, M.E., Cotter, A.M., 2015. Fish tissue lipid-C:n relationships for correcting δ^{13}C values and estimating lipid content in aquatic food-web studies. Rapid Commun. Mass. Sp. 29, 2069–2077.

Hong, Y., Hull, P., Rifkin, E., Bouwer, E.J., 2013. Bioaccumulation and biomagnification of mercury and selenium in the Sarasota Bay ecosystem. Environ. Toxicol. Chem. 32, 1143–1152.

Huang, S., Jiang, R., Song, Q., Zhang, Y., Huang, Q., Su, B., Chen, Y., Huo, Y., Lin, H., 2020. Study of mercury transports and transformation in mangrove forests using stable mercury isotopes. Sci. Total Environ. 704, 135928.

Huang, S., Zhao, Y., Lv, S., Wang, W., Wang, W., Zhang, Y., Huo, Y., Sun, X., Chen, Y., 2021. Distribution of mercury isotope signatures in Yundang Lagoon, Xiamen, China, after long-term interventions. Chemosphere 272, 129716.

Huber, J., Heimburger, L.E., Sonke, J.E., Ziller, S., Lindén, M., Leopold, K., 2015. Nanogold-decorated silica monoliths as highly efficient solidphase adsorbent for ultra-trace mercury analysis in natural waters. Anal. Chem. 87, 11122–11129.

Jiskra, M., Heimbürger-Boavida, L., Desgranges, M., Petrova, M.V., Dufour, A., Ferreira-Araujo, B., Masbou, J., Chmeleff, J., Thyssen, M., Point, D., Sonke, J.E., 2021. Mercury stable isotopes constrain atmospheric sources to the ocean. Nature 597, 678–682.

Jiskra, M., Wiederhold, J.G., Skyllberg, U., Kronberg, R.M., Kretzschmar, R., 2017. Source tracing of natural organic matter bound mercury in boreal forest runoff with mercury stable isotopes. Environ. Sci. Proc. Imp. 18, 1235–1248.

Kim, H., Kumar, K.S., Shin, K.H., 2015. Applicability of stable C and N isotope analysis in inferring the geographical origin and authentication of commercial fish (Mackerel, Yellow Croaker and Pollock). Food Chem. 172, 523–527.

Krabbenhoft, D.P., Sunderland, E.M., 2013. Global change and mercury. Science 341, 1457–1458.

Kritee, K., Barkay, T., Blum, J.D., 2009. Mass dependent stable isotope fractionation of mercury during mer mediated microbial degradation of monomethylmercury. Geochim. Cosmochim. Acta 73, 1285–1296.

Kwon, S.Y., Blum, J.D., Yin, R.S., Tsui, M.T.K., Yang, Y.H., Choi, J.W., 2020. Mercury stable isotopes for monitoring the effectiveness of the Minamata Convention on Mercury. Earth Sci. Rev. 203, 103111.
Lamborg, C.H., Hammerschmidt, C.R., Bowman, K.L., Swarr, G.J., Munson, K.M., Ohnemus, D.C., Lam, P.J., Heimbürger, L., Rijkenberg, M.J.A., Saito, M.A., 2014. A global ocean inventory of anthropogenic mercury based on water column measurements. Nature 512, 65–68.
Lamborg, C.H., Yiğiterhan, O., Fitzgerald, W.F., Balcom, P.H., Hammerschmidt, C.H., Murray, J., 2008. Vertical distribution of mercury species at two sites in the western Black Sea. Mar. Chem. 28, 77–89.
Lepak, R.F., Janssen, S.E., Yin, R., Krabbenhoft, D.P., Ogorek, J.M., DeWild, J.F., Tate, M. T., Holsen, T.M., Hurley, J.P., 2018. Factors affecting mercury stable isotopic distribution in piscivorous fish of the Laurentian Great Lakes. Environ. Sci. Technol. 52, 2768–2776.
Lepak, R.F., Ogorek, J.M., Bartz, K.K., Janssen, S.E., Tate, M.T., Runsheng, Y., Hurley, J. P., Young, D.B., Eagles-Smith, C.A., Krabbenhoft, D.P., 2022. Using carbon, nitrogen, and mercury isotope values to distinguish mercury sources to Alaskan Lake trout. Environ. Sci. Tech. Let. 9, 312–319.
Li, K., Lin, C.J., Yuan, W., Sun, G., Fu, X., Feng, X., 2019. An improved method for recovering and preconcentrating mercury in natural water samples for stable isotope analysis. J. Anal. At. Spectrom. 34, 2303–2313.
Liu, C.B., Hua, X.B., Liu, H.W., Yu, B., Mao, Y.X., Wang, D.Y., Yin, Y.G., Hu, L.G., Shi, J. B., Jiang, G.B., 2018. Tracing aquatic bioavailable Hg in three different regions of China using fish Hg isotopes. Ecotox. Environ. Safe. 150, 327–334.
Liu, J., Xu, X., Yu, S., Cheng, H., Hong, Y., Feng, X., 2014. Mercury pollution in fish from South China Sea: levels, species-specific accumulation, and possible sources. Environ. Res. 131, 160–164.
Liu, M., Zhang, Q., Maavara, T., Liu, S., Wang, X., Raymond, P.A., 2021a. Rivers as the largest source of mercury to coastal oceans worldwide. Nat. Geosci. 14, 672–677.
Liu, Y., Chen, J., Liu, J., Gai, P., Yang, D.A., Zheng, W., Li, Y., Li, D., Cai, H., Yuan, W., Li, Y., 2021b. Coprecipitation of mercury from natural iodine-containing seawater for accurate isotope measurement. Anal. Chem. 93, 15905–19512.
Madigan, D.J., Li, M., Yin, R., Baumann, H., Snodgrass, O.E., Dewar, H., Krabbenhoft, D. P., Baumann, Z., Fisher, N.S., Balcom, P., Sunderland, E.M., 2018. Mercury stable isotopes reveal influence of foraging depth on mercury concentrations and growth in Pacific bluefin tuna. Environ. Sci. Technol. 52, 6256–6264.
Mason, R.P., Choi, A.L., Fitzgerald, W.F., Hammerschmidt, C.R., Lamborg, C.H., Soerensen, A.L., Sunderland, E.M., 2012. Mercury biogeochemical cycling in the ocean and policy implications. Environ. Res. 119, 101–117.
Maurice, L., Croizier, G.L., Morales, G., Carpintero, N., Guayasamin, J.M., Sonke, J., Paez-Rosas, D., Point, D., Bustos, W., Ochoa-Herrera, V., 2021. Concentrations and stable isotopes of mercury in sharks of the Galapagos Marine Reserve: human health concerns and feeding patterns. Ecotox. Environ. Safe. 215, 112122.
Meng, M., Sun, R.Y., Liu, H.W., Yu, B., Yin, Y.G., Hu, L.G., Chen, J.B., Shi, J.B., Jiang, G. B., 2020. Mercury isotope variations within the marine food web of Chinese Bohai Sea: implications for mercury sources and biogeochemical cycling. J. Hazard. Mater. 384, 121379.
Motta, L.C., Blum, J.D., Popp, B.N., Umhau, B.P., Benitez-Nelson, C.R., Close, H.G., Washburn, S.J., Drazen, J.C., 2022. Mercury isotopic evidence for the importance of particles as a source of mercury to marine organisms. P. Natl. Acad. Sci. USA 119, e2208183119.
Perrot, V., Landing, W.M., Grubbs, R.D., Salters, V.J.M., 2019. Mercury bioaccumulation in tilefish from the northeastern Gulf of Mexico 2 years after the Deepwater Horizon oil spill: insights from Hg, C, N and S stable isotopes. Sci. Total Environ. 666, 828–838.
Peterson, B.J., Fry, B., 1987. Stable isotopes in ecosystem studies. Annu. Rev. Ecol. Syst. 18, 293–320.
Schartup, A.T., Thackray, C.P., Qureshi, A., Dassuncao, C., Gillespie, K., Hanke, A., Sunderland, E.M., 2020. Climate change and overfishing increase neurotoxicant in marine predators. Nature 572, 1–3.
Senn, D.B., Chesney, E.J., Blum, J.D., Bank, M.S., Maage, A., Shine, J.P., 2010. Stable isotope (N, C, Hg) study of methylmercury sources and trophic transfer in the Northern Gulf of Mexico. Environ. Sci. Technol. 44, 1630–1637.
Smith, C.N., Kesler, S.E., Blum, J.D., Rytuba, J.J., 2008. Isotope geochemistry of mercury in source rocks, mineral deposits and spring deposits of the California coast ranges. USA. Earth Planet. Sci. Lett. 269, 399–407.
Sun, R.Y., Yuan, J.J., Sonke, J.E., Zhang, Y.X., Zhang, T., Zheng, W., Chen, S., Meng, M., Chen, J.B., Liu, Y., 2020. Methylmercury produced in upper oceans accumulates in deep Mariana Trench fauna. Nat. Commun. 11, 3389–3397.
Tsui, M.T.K., Blum, J.D., Kwon, S.Y., 2020a. Review of stable mercury isotopes in ecology and biogeochemistry. Sci. Total Environ. 716, 135386.
Tsui, M.T.K., Kwon, S.Y., Li, M.L., Bishop, K., 2022. Comments on "Decreasing mercury levels in consumer fish over the three decades of increasing mercury emissions in China". Eco Environ. Health 1, 46–52.
Tsui, M.T.K., Uzun, H., Ruecker, A., Majidzadeh, H., Ulus, Y., Zhang, H., Bao, S., Blum, J. D., Karanfil, T., Chow, A.T., 2020b. Concentration and isotopic composition of mercury in a blackwater river affected by extreme flooding events. Limnol. Oceanogr. 65, 2158–2169.
Wang, C., Wang, Z., Zhang, X., 2020. Characteristics of mercury speciation in seawater and emission flux of gaseous mercury in the Bohai Sea and Yellow Sea. Environ. Res. 182, 109092.
Wang, J., Tong, Y., Feng, L., Zhao, D., Zheng, C., Tang, J., 2021. Satellite-observed decreases in water turbidity in the Pearl River Estuary: potential linkage with sea-level rise. J. Geophys. Res. Oceans 126, e2020JC016842.
Wang, Y., Yu, X., Xu, J., 2011. Decreased trophic position as a function of increasing body size of a benthic omnivorous fish from the largest freshwater lake in China. Environ. Biol. Fish. 91, 505–512.
Wiederhold, J.G., Cramer, C.J., Daniel, K., Infante, I., Bourdon, B., Kretzschmar, R., 2010. Equilibrium mercury isotope fractionation between dissolved Hg(II) species and thiol-bound Hg. Environ. Sci. Technol. 44, 4191–4197.
Woerndle, G.E., Tsui, M.T.K., Sebestyen, S.D., Blum, J.D., Nie, X., Kolka, R.K., 2018. New insights on ecosystem mercury cycling revealed by stable isotopes of mercury in water flowing from a headwater peatland catchment. Environ. Sci. Technol. 52, 1854–1861.
Xia, J., Wang, J., Zhang, L., Wang, X., Yuan, W., Peng, T., Zheng, L., Tian, W., Feng, X., 2022. Migration and transformation of soil mercury in a karst region of southwest China: implications for groundwater contamination. Water Res 226, 119271.
Xu, X.Y., Zhang, Q.G., Wang, W.X., 2016. Linking mercury, carbon, and nitrogen stable isotopes in Tibetan biota: implications for using mercury stable isotopes as source tracers. Sci. Rep. 6, 25394.
Yan, J., Li, R., Ali, M.U., Wang, C., Wang, B., Jin, X., Shao, M., Li, P., Zhang, L., Feng, X., 2023. Mercury migration to surface water from remediated mine waste and impacts of rainfall in a karst area-Evidence from Hg isotopes. Water Res. 230, 119592.
Yang, S., Sun, K., Liu, J., Wei, N., Zhao, X., 2022. Comparison of pollution levels, biomagnification capacity, and risk assessments of heavy metals in nearshore and offshore regions of the South China Sea. Int. J. Environ. Res. Pub. He. 19, 12248.
Yang, S., Wang, B., Qin, C., Yin, R., Li, P., Liu, J., Point, D., Maurice, L., Sonke, J.E., Zhang, L., Feng, X., 2021. Compound-specific stable isotope analysis provides new insights for tracking human monomethylmercury exposure sources. Environ. Sci. Technol. 55, 12493–12503.
Yin, R., Feng, X., Chen, B., Zhang, J., Wang, W., Li, X., 2015. Identifying the sources and processes of mercury in subtropical estuarine and ocean sediments using Hg isotopic composition. Environ. Sci. Technol. 49, 1347–1355.
Yin, R., Feng, X., Zhang, J., Pan, K., Wang, W., Li, X., 2016. Using mercury isotopes to understand the bioaccumulation of Hg in the subtropical Pearl River Estuary, South China. Chemosphere 147, 173–179.
York, D., Evensen, N.M., Martinez, M.L., Delgado, D.B., 2004. Unified equations for the slope, intercept, and standard errors of the best straight line. Am. J. Phys. 72, 367–375.
Yu, X.J., Yan, Y., Wang, W.X., 2010. The distribution and speciation of trace metalsin surface sediments from the Pearl River estuary and the Daya Bay, southern China. Mar. Pollut. Bull. 60, 1364–1371.
Zhan, W., Yao, Y., Zhang, Z., Sun, Z., Zhan, M., Sun, L., Liu, Z., 2006. Crustal activities recorded in coral reefs in the northwestern South China Sea. Chin. Sci. Bull. 51 (Supp. II), 89–94.
Zhang, M., Wu, Y., Qi, L., Xu, M., Yang, C., Wang, X., 2019. Impact of the migration behavior of mesopelagic fishes on the compositions of dissolved and particulate organic carbon on the northern slope of the South China Sea. Deep-Sea Res. Pt. II 167, 46–54.
Zhang, Y., Chen, J., Zheng, W., Sun, R., Yuan, S., Cai, H., Yang, D.A., Yuan, W., Meng, M., Wang, Z., Liu, Y., Liu, J., 2020. Mercury isotope compositions in large anthropogenically impacted Pearl River, South China. Ecotoxicol. Environ. Safe. 191, 110229.